Cell Reports, Volume *28*

Supplemental Information

Structural Disconnections Explain Brain Network Dysfunction after Stroke

Joseph C. Griffis, Nicholas V. Metcalf, Maurizio Corbetta, and Gordon L. Shulman

Supplementary Material

Table S1. Demographic information. Related to STAR Methods

Group	Age (Mean/SD)	Sex	Handedness	Education (Mean/SD)	Lesion Side
Patients (N=114)	52.4/10.2	58 F, 56 M	106 R, 8 L	13.3/2.8	54 R, 60 L
Controls (N=24)	54.5/13.5	12 F, 12 M	23 R, 1 L	13.5/2.1	N/A

SD: Standard Deviation, M: Male, F: Female, R: Right, L: Left

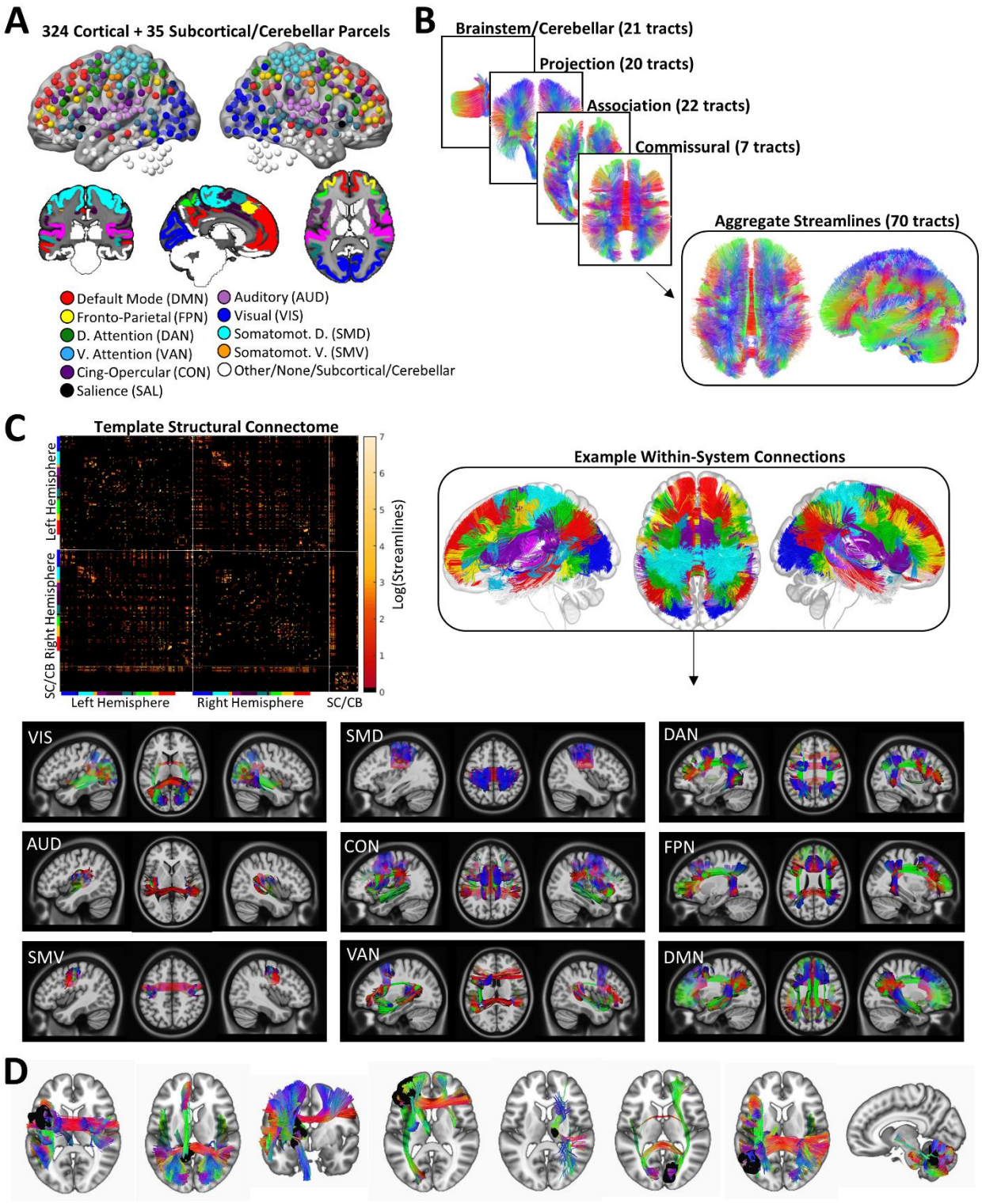

Figure S1. Related to Figure 1; STAR Methods; Structural data. A. Spheres centered on the centroid co-ordinates of the 359 grey matter regions are color-coded by network affiliations. Orthogonal slices below show volume-space regions including subcortical and cerebellar regions. **B.** Curated streamlines corresponding to 70 macroscale fiber pathways were combined into a single tractography atlas. **C.** The grey

matter regions and tractography atlas were used to construct a template structural connectome using endpoint-to-endpoint streamline extraction. The matrix shows the template structural connectome, and the colorscale corresponds to log(streamlines). The tractography image shows the within-network structural connections for the cortical networks shown in (A). Illustrations of structural connections for individual networks are shown below. Note that between-networks connections are not shown despite being numerous. **D.** Example disconnections for 8 patients with heterogeneous lesions. Lesions are shown in black.

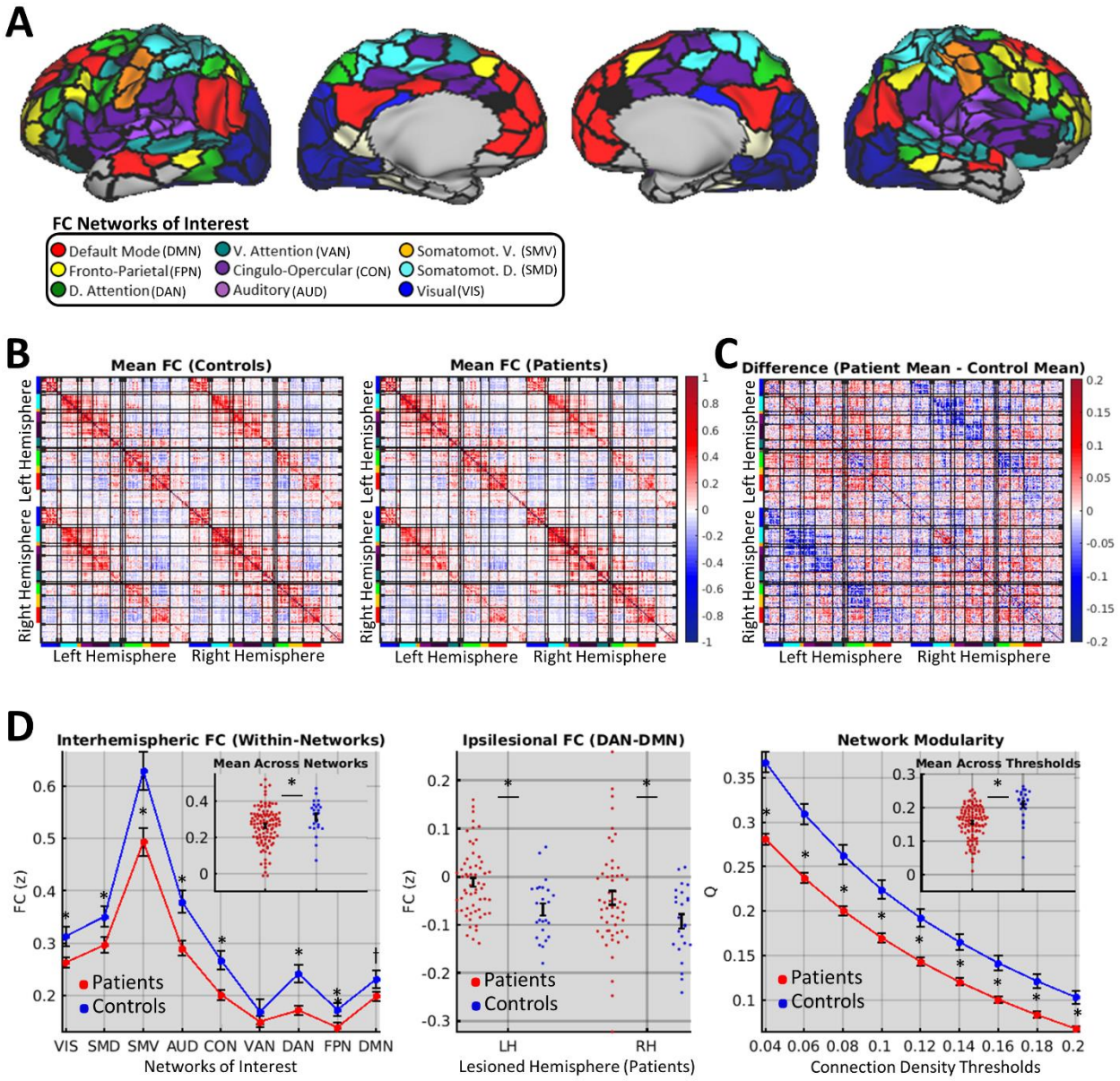

Figure S2. Related to Figures 2-7; STAR Methods -- Quantification and Statistical Analyses – Functional connectivity measures; Functional connectivity disruptions in sub-acute stroke. A. Cortical regions color-coded by network (see also **Fig. S1**). **B.** Mean FC matrices for the control group (*n*=24, left) and patient group (*n*=114, right). Colored bars on axes indicate FC networks shown in (A) and are organized by hemisphere such that the upper left and lower right quadrants respectively correspond to connections within the left and right hemispheres, while bottom left and upper right quadrants correspond to interhemispheric connections. **C.** Difference between matrices in (B). **D.** Summary measures for patients (*n*=114, red) and controls (*n*=24, blue). Left – interhemispheric within-network FC (y-axis) for each of the nine networks of interest (x-axis) for patients (red) and controls (blue). Middle – ipsilesional DAN-DMN FC values for patients with left hemispheric (red; LH) and right hemispheric (red; RH) lesions, and values from the corresponding hemisphere in controls (blue).

Plots show means/standard errors. Right – FC modularity (y-axis) for patients (red) and controls (blue) computed across a range of different connection density thresholds (x-axis). *two-sample *t*-test FDRp<0.05.

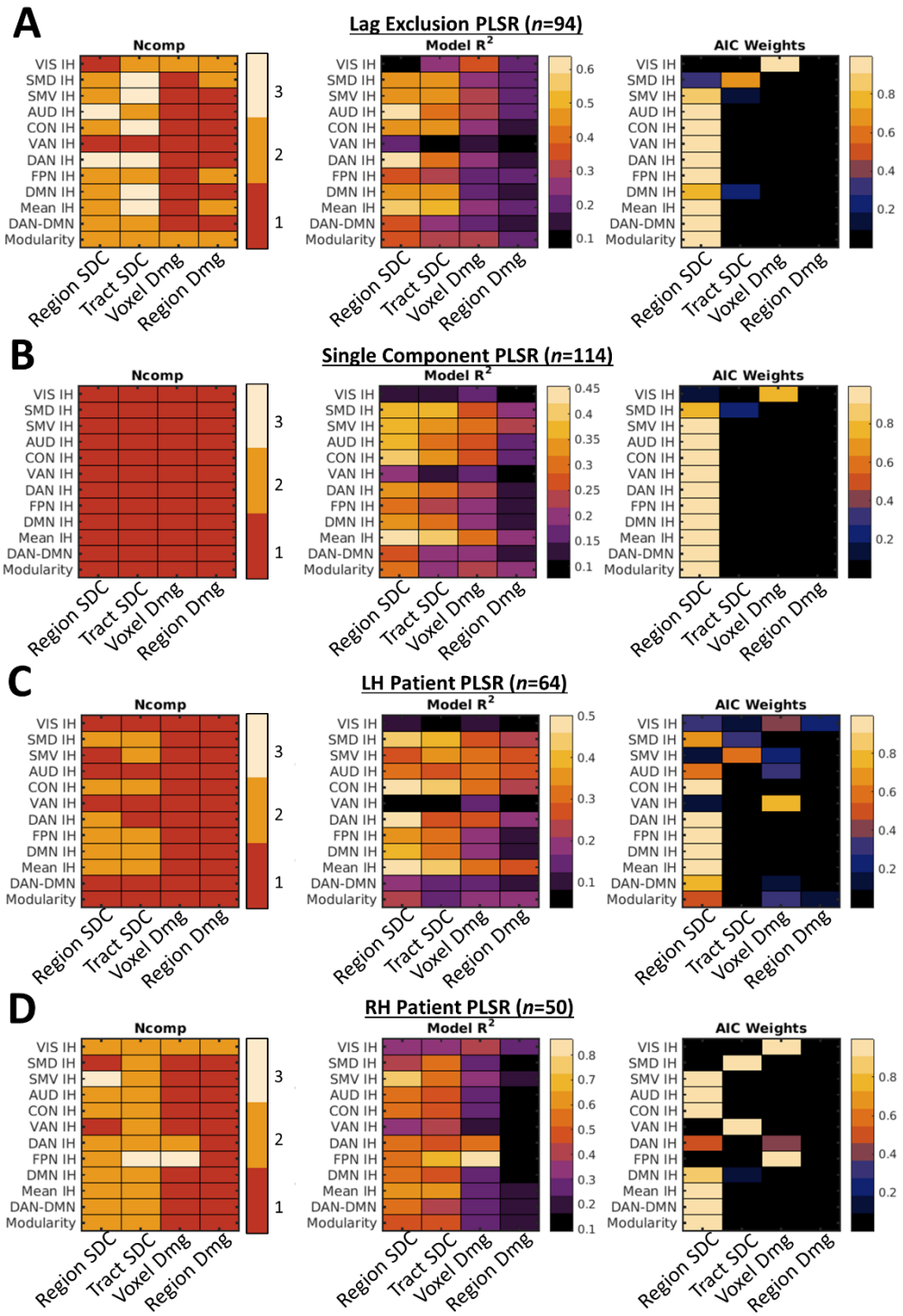

Figure S3. Related to Figure 3. Additional PLSR Analyses. A-D. Matrices show the number of components per PLSR model (left), PLSR model fits (middle), and PLSR AIC weights (right) from PLSR analyses where **(A)** analyses were restricted to the subset of patients with mean hemispheric lag differences less than 2 SD from the control mean (*n*=94 out of 114), **(B)** analyses were run such that each model only included 1 component using data from the full patient group (*n*=114), **(C)** analyses were restricted

to the subset of patients with left hemispheric (LH) lesions (*n*=60 out of 114), and **(D)** analyses were restricted to patients with right hemispheric (RH) lesions (*n*=54 out of 114). All analyses produced results that were highly consistent with the results obtained from the main analyses. Nearly identical results were also obtained even when lesioned vertices were included in the FC measures (not shown).

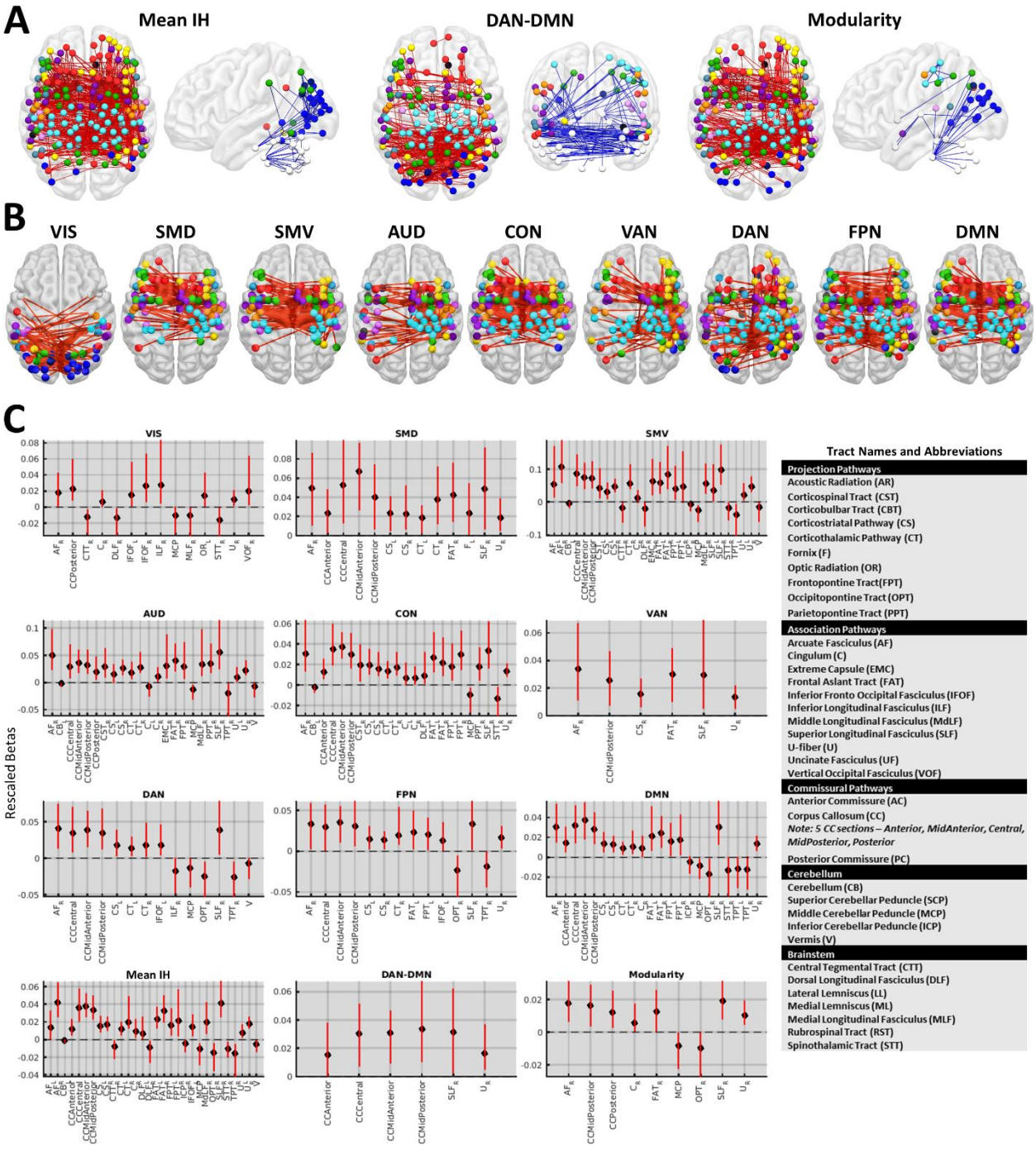

Figure S4. Related to Figure 4. PLSR SDC model weights. A. PLSR model weights for region-based SDCs from analyses of data from the full patient group (*n*=114). The top row shows the full PLSR weight topographies (i.e. all positive and negative weights with significant 99% CIs) for the three primary measures of interest (see **Figure 4**) from analyses of the patient group. The bottom row shows the top 20% of positive PLSR region-based SDC model weights with significant 99% CIs for the models of network-specific interhemispheric FC. Images include both interhemispheric and intrahemispheric disconnections. **B.** PLSR tract-based SDC model weights with

significant 99% CIs from analyses of data from the full patient group (*n*=114). Error bars correspond to 99% CIs as estimated via the bias-corrected and percentile-accelerated method. Tract names and abbreviations are provided in the legend. Weights are coded such that positive weights predict more severe disruptions of each FC measure, and negative weights predict less severe disruptions of each FC measure.

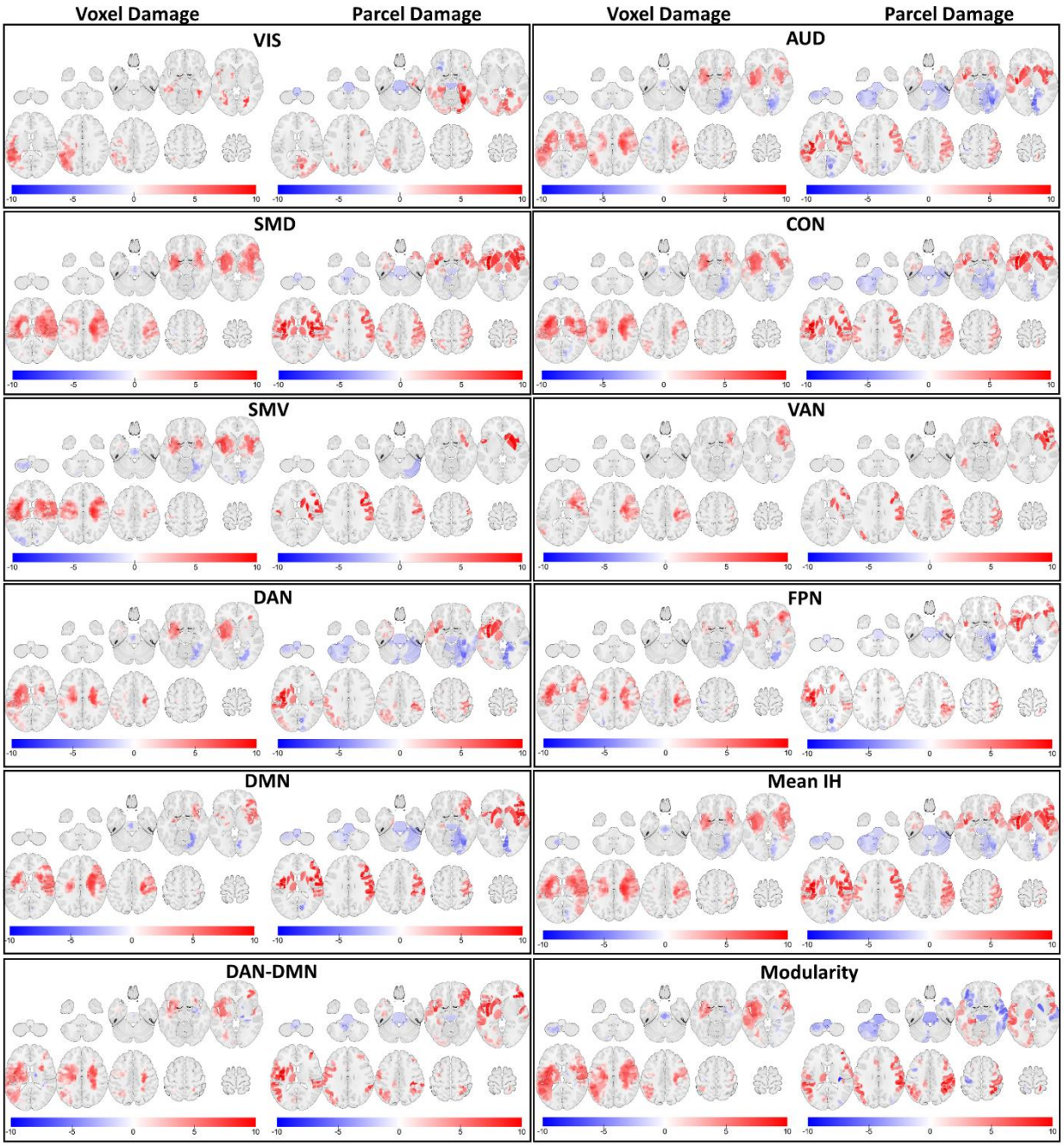

Figure S5. Related to Figure 4. Voxel-based and region-based damage PLSR model weights. PLSR voxel-based damage and region-based damage model weights with significant 99% CIs are shown for each model fit from analyses of the full the patient group (*n*=114). Weights are coded such that positive weights predict more severe disruptions of each FC measure, and negative weights predict less severe disruptions of each FC measure. Note that voxel-based damage weights emphasize white matter damage, but that white matter effects appear to be displaced into nearby cortical areas in the region-based damage maps.

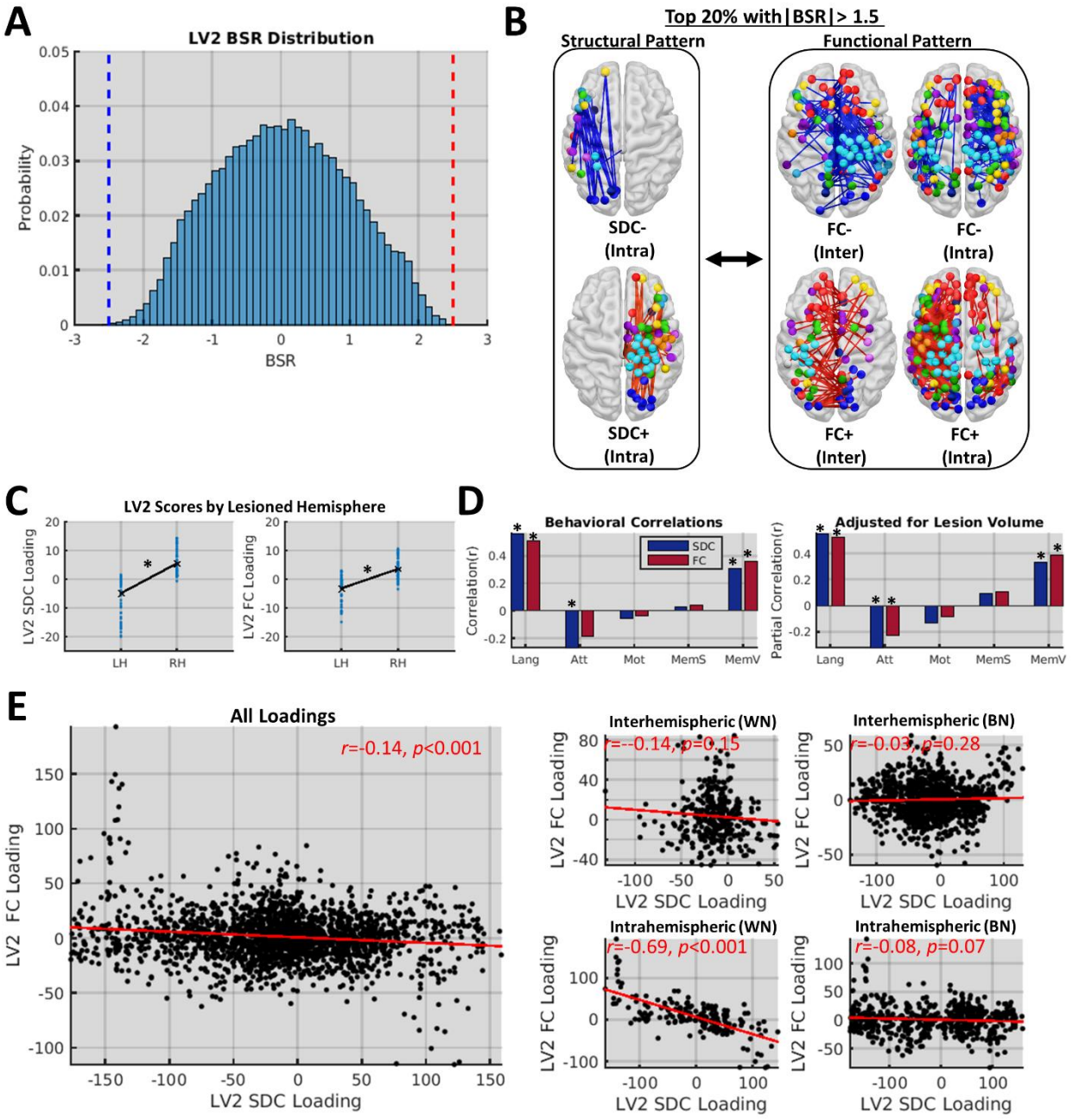

Figure S6. Related to Figure 5. Characterization of PLSC LV2. A. The histogram shows the distribution of BSRs for LV2 (i.e. both SDC and FC BSRs) from the PLSC analyses of the full patient group (*n*=114). The dashed lines correspond to the significance thresholds (i.e. BSRs > 2.5, BSRs < -2.5) used in the main analyses. Loadings were not sufficiently stable to survive the significance threshold used for the main analyses. **B.** To illustrate the general patterns captured by LV2, the top 20% of positive and negative loadings with |BSRs| > 1.5 are shown. SDC loadings on LV2 only included intrahemispheric edges, and loading signs differed for left vs. right hemispheric SDCs. FC loadings are shown separately for interhemispheric (left) and intrahemispheric (right) edges. FC loadings largely corresponded to intrahemispheric

functional connections contralateral to SDCs with the same sign. Thus, LV2 appeared to primarily capture negative covariation between intrahemispheric SDCs and contralateral intrahemispheric FC. That is, less intrahemispheric SDCs within a given hemisphere were associated with stronger FC within that hemisphere, while more intrahemispheric SDCs within a given hemisphere were associated with weaker FC within that hemisphere. Interhemispheric functional connections largely featured midline regions and regions associated with somatomotor and default mode networks. Node network assignments are color coded as in **Figure S1**. **C.** While expression of LV2 differed significantly between subsets of patients with left (n=60) vs. right hemispheric (n=54) lesions (SDC: t_{112}=-9.74, p<0.001; FC: t_{112}=-8.85, p<0.001), it was not a strict recapitulation of lesion side (SDC: R^2=0.46; FC: R^2=0.41); patients with lesions in a given hemisphere still varied with respect to how much LV2 was expressed in their data. **D.** The expression of LV2 significantly correlated with deficits in language, attention, and memory domains across the full patient group (n=114), even when adjusting for lesion size, indicating that it was also behaviorally relevant. **E.** Weak but significant topographical similarity was observed between the unthresholded LV2 SDC and FC weight vectors obtained from PLSC analysis of data from the full patient group (n=114). *FDRp<0.05.

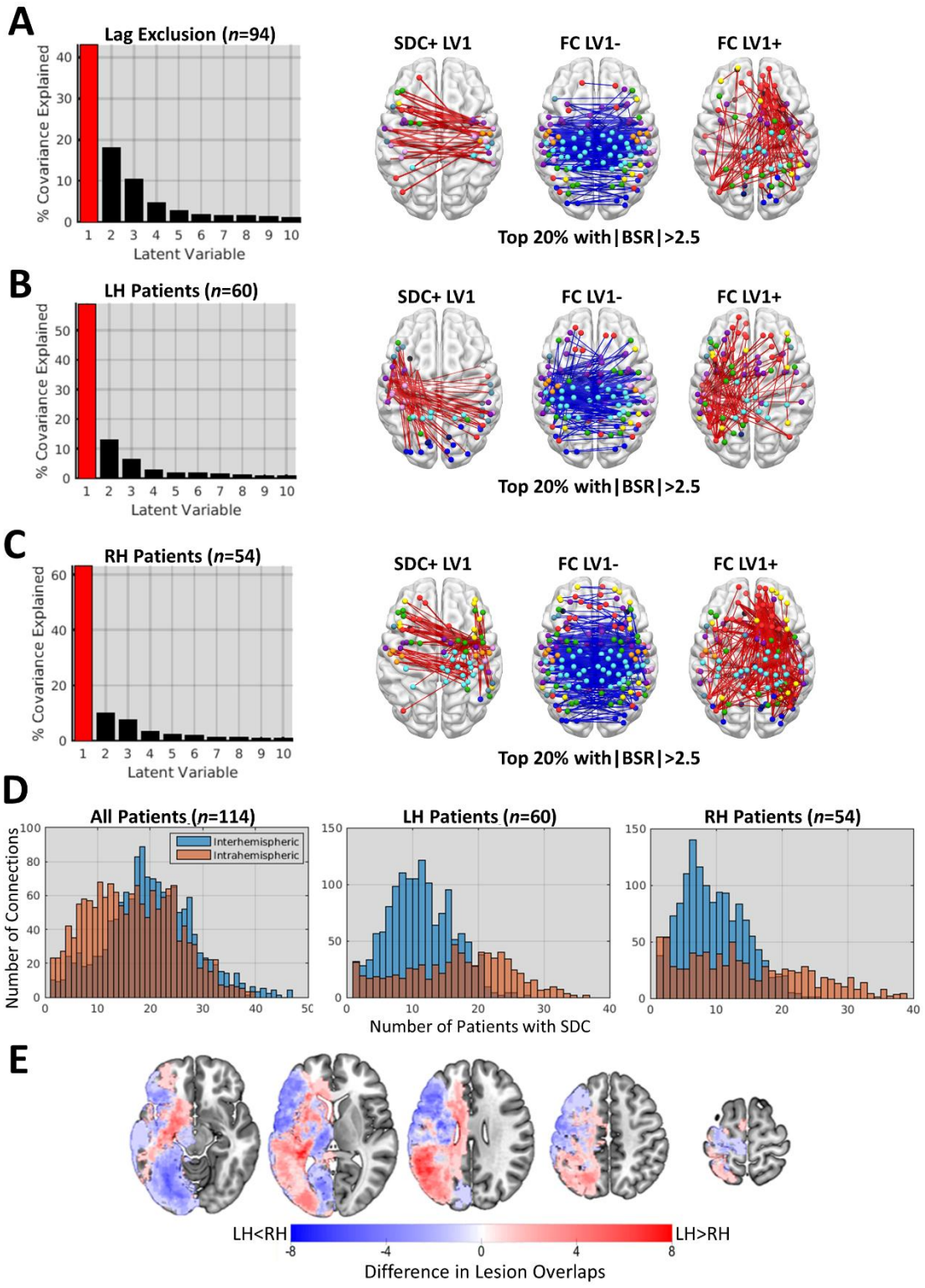

Figure S7. Related to Figure 5; STAR Methods – Quantification and Statistical Analyses – Additional Analyses. Supplemental PLSC Analyses. A-C. The scree plots show the first 10 LVs obtained from PLSC analyses where **(A)** analyses were restricted to the subset of patients with mean hemispheric lag differences less than 2

SD from the control mean (*n*=94 out of 114), **(B)** analyses were restricted to the subset of patients with left hemispheric (LH) lesions (*n*=60 out of 114), and **(C)** analyses were restricted to the subset of patients with right hemispheric (RH) lesions (*n*=54 out of 114). The brain plots show the top 20% of significant PLSC loadings from each analysis. **D.** The top FC loadings obtained from the separate subgroup analyses shown in **B-C** closely resembled the FC pattern reported in the full group analyses (*n*=114) in the main text (see **Fig. 5D**, functional pattern), but the top SDC loadings from the separate subgroup group analyses shown in **B-C** differed from the SDC pattern reported in the full group analyses (*n*=114) in main text (see **Fig. 5D**, structural pattern) as they included both interhemispheric and intrahemispheric connections. We reasoned that the inclusion of intrahemispheric connections might reflect a bias towards intrahemispheric SDC effects in the LH-only and RH-only subgroup analyses. Such a bias might be expected if across-patient overlaps were higher for intrahemispheric SDCs than for interhemispheric SDCs within each group, but not when the groups were combined (i.e. due to interhemispheric SDCs being possible for patients in either group). To assess whether this was the case, we plotted the across-patient overlaps for interhemispheric (IH – blue) and intrahemispheric (WH – orange) SDCs from each analysis. The histograms show the number of connections (y-axes) with different numbers of overlapping SDCs across patients (i.e. x-axes) in the analyses that included all patients (left), LH patients (middle), and RH patients (right). Inter- and intrahemispheric SDC overlap distributions are most similar for the analysis of all patients (left). This suggests that the inclusion of intrahemispheric SDCs in the top weight maps from the separate subgroup analyses shown in **(B-C)** likely reflects a bias towards intrahemispheric SDC effects in the separate subgroup analyses of LH and RH patients, and suggests that the analyses of the full patient sample were least likely to be biased towards a particular type of SDC effect. **E.** The top SDC loadings obtained from the separate subgroup analyses in **(B-C)** differed topographically in that the top loadings for LH patients included more posterior connections while the top loadings for RH patients included more frontal connections. We considered it likely that these differences might reflect differences in the lesion topographies of LH and RH patient groups. To verify this, we created voxel-based damage maps for each group and flipped the map for the RH group to the left hemisphere. We then subtracted the RH map from the LH map to obtain the map shown in **(E)**. Blue voxels were damaged more frequently in patients with RH lesions, while red voxels were damaged more frequently in patients with LH lesions. Group differences in top SDC loading topographies shown in **(B-C)** largely appear to reflect differences in damage topographies between groups, consistent with our expectation.

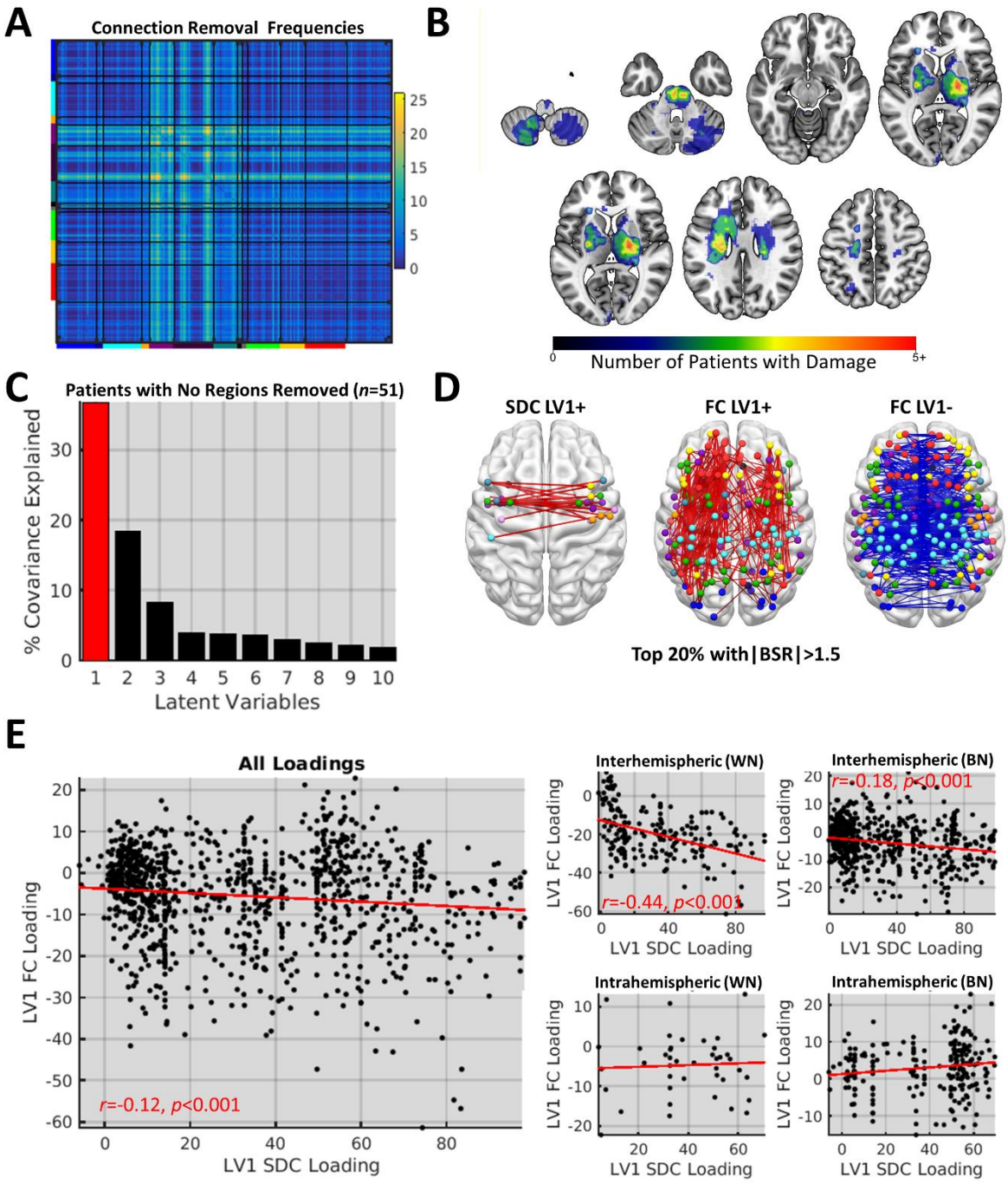

Figure S8. Related to Methods – Quantification and Statistical Analyses – Additional Analyses. Related to Figures 5 and 7. Results from PLSC analyses of patients with no regions removed. A. The matrix shows the number of patients for whom each connection was removed. **B.** Voxel-based damage overlaps are shown for a subset (*n*=51 out of 114) patients who did not have any regions that were sufficiently damaged to be removed. **C.** The scree plot shows the results of a PLSC analysis performed on the subset 51 patients with no regions removed. **D.** The brain images show the top 20% of positive and negative SDC and FC loadings that survived a relaxed threshold of |BSR|>1.5 as few loadings survived at the threshold used in the

main analyses. **E.** The left scatterplot shows the relationship between all connections with non-zero LV1 SDC and FC loadings in the subset of 51 patients with no regions removed. The right scatterplots show the relationships between LV1 SDC and FC loadings for different connection types. While intrahemispheric within-network SDC and FC loadings were no longer significantly correlated, this was likely due to the small number of intrahemispheric within-network SDCs in this subsample. The significant correlations between interhemispheric/intrahemispheric between-network SDC and FC loadings may reflect the specific connections included in this sample. Despite these differences, these results argue that the topographic similarity between the SDC and FC loadings is not due to the removal of heavily damaged regions from the FC matrices.

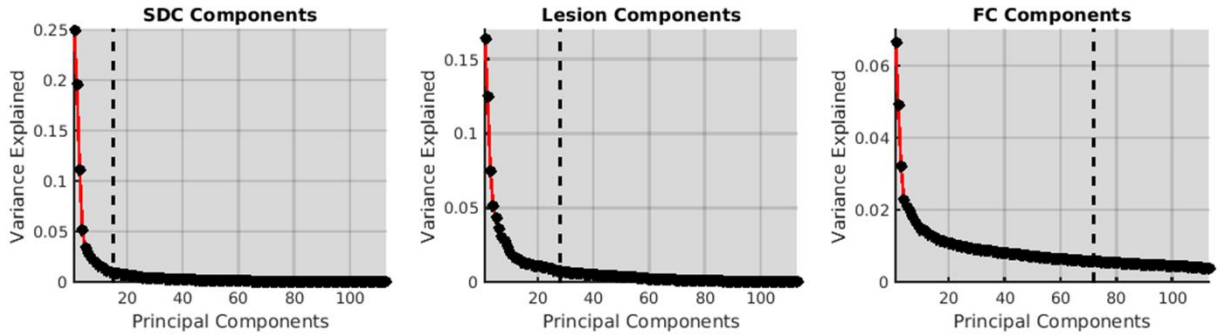

Figure S9. Related to Methods – Quantification and Statistical Analyses – Additional Analyses. Dimensionality of SDC, lesion, and FC data. Scree plots showing the proportion of variance explained by principal components of the region-based SDC (left), voxel-based daamge (middle), and FC (right) data from the full patient sample (*n=114*). Dashed lines correspond to the number of components needed to explain 80% of the variance in each dataset. All datasets exhibited much higher dimensionality than the covariance between the SDC and FC datasets.